FFI RAPPORT

THE IMPACT OF FLOW NOISE ON TOWED AND HULL MOUNTED ACOUSTICAL SENSORS - AN INTRODUCTORY STUDY

REIF Bjørn A P, ANDREASSEN Øyvind

FFI/RAPPORT-2004/00858

THE IMPACT OF FLOW NOISE ON TOWED AND HULL MOUNTED ACOUSTICAL SENSORS - AN INTRODUCTORY STUDY

REIF Bjørn A P, ANDREASSEN Øyvind

FFI/RAPPORT-2004/00858

FORSVARETS FORSKNINGSINSTITUTT
Norwegian Defence Research Establishment
P O Box 25, NO-2027 Kjeller, Norway

FORSVARETS FORSKNINGSINSTITUTT (FFI)
Norwegian Defence Research Establishment

P O BOX 25
N0-2027 KJELLER, NORWAY

UNCLASSIFIED

SECURITY CLASSIFICATION OF THIS PAGE
(when data entered)

REPORT DOCUMENTATION PAGE

1) PUBL/REPORT NUMBER	2) SECURITY CLASSIFICATION	3) NUMBER OF PAGES
FFI/RAPPORT-2004/00858	UNCLASSIFIED	35
1a) PROJECT REFERENCE	**2a) DECLASSIFICATION/DOWNGRADING SCHEDULE**	
FFI-IV/416501	-	

4) TITLE

THE IMPACT OF FLOW NOISE ON TOWED AND HULL MOUNTED ACOUSTICAL SENSORS - AN INTRODUCTORY STUDY

5) NAMES OF AUTHOR(S) IN FULL (surname first)

REIF Bjørn A P, ANDREASSEN Øyvind

6) DISTRIBUTION STATEMENT

Approved for public release. Distribution unlimited. (Offentlig tilgjengelig)

7) INDEXING TERMS

IN ENGLISH:	IN NORWEGIAN:
a) Turbulent boundary layers	a) Turbulente grensesjikt
b) Wall pressure fluctuations	b) Vegg-trykks fluktuasjoner
c) Flow induced noise	c) Strømningsindusert støy
d) Turbulent wakes	d) Turbulente kjølvann
e)	e)

THESAURUS REFERENCE:

8) ABSTRACT

In this introductory study we have assessed the impact of turbulence generated wall-pressure fluctuations on surface-mounted acoustical sensors, with a special focus on towed sonar arrays. The main findings are that the sound-pressure-levels generally can be expected to be broad banded and exhibit very high SPLs, even at low towing speeds. The SPLs increases dramatically with increased towing speed. By increased the sensor area, the pressure-fluctuations on the surface are convolved such that the SPL decreases. Some brief discussions on transfers of waves within towed antennas are also included, together with some comments on the downstream evolution of a submarine wake and its interaction with a towed antenna.

The results of this study show that turbulence generated flow noise on towed, or hull-mounted, acoustical sensors are significant. It is therefore seems necessary to further address this problem in order to understand how flow noise affects these systems which necessarily has an adverse impact on the performance. Such a fundamental study would enable advanced signal processing routines to be tested and further developed, parametric studies concerning optimal design to be conducted as so forth.

9) DATE	AUTHORIZED BY	POSITION
	This page only	
2004-03-02	John Mikal Størdal	Director

ISBN-82-464-0827-5

UNCLASSIFIED

SECURITY CLASSIFICATION OF THIS PAGE
(when data entered)

CONTENTS

THE IMPACT OF FLOW NOISE ON TOWED AND HULL MOUNTED ACOUSTICAL SENSORS - AN INTRODUCTORY STUDY

1 INTRODUCTION

The terminology ’flow noise’ used throughout this report alludes to the impact of turbulent fluid motion on towed or hull mounted sensors. More precisely it deals primarily with the dynamical nature of pressure fluctuations *on the surface of the antenna or hull*. These are generated by the fluctuating turbulent motion of water (or air) passing by the surface itself. The radiation of sound from the boundary layer into the freestream is thus not considered, nor the propagation of sound from the surface through the interior of the antenna (or inside the hull).

This introductory study is based on a rather extensive literature survey of readily available non-classified literature. Although the main focus of attention is on towed sonar arrays, the study is of such a general nature that the conceptual methodology easily can be applied to hull mounted sensors on ships, submarines or aircrafts.

We will pay special attention to the towed acoustical array proposed for the Ula class submarine. The design of a this system is currently ongoing. For various technical reasons it is proposed that the array will be towed within the submarine wake flow field. The generation and evolution of a submarine wake will be discussed as well as the impact of the wake flow field on the fluid dynamical fluctuations on the antenna surface.

Some recent work has been done at FFI in order to evaluate towed array performance, but we are not aware of any previous FFI studies that have addressed the problem of flow noise in conjunction with towed or hull mounted sensors - a research topic that currently is receiving much attention internationally.

1.1 Outline of the study

It has been necessary to limit the scope of the present report, and the main contents of the study can be outlined as follows:

- A discussion of pressure fluctuations and their relation to sound pressure levels caused by the antenna boundary layer in a quiescent (smooth) fluid environment.
- A discussion of the submarine wake/array boundary-layer interactions.
- A qualitative estimate of the effect of towing speed on the generation of flow noise.
- A qualitative estimate of the effect of convolution of turbulence and the aperture of the hydrophones.

- Recommendations for further studies.

2 FLOW INDUCED NOISE

There are several sources of noise relevant for a towed sonar array system, and some of these are discussed in this section. In addition to a so-called *hydrostatic contribution*, which originates from structural vibrations, there are two primary *dynamical contributions* that are considered here; (i) the boundary layer created by the antenna itself when it moves relative to the surrounding water, and (ii) the dynamic effects of the submarine wake. We will mainly focus our attention on the simplest possible scenario, namely an antenna that is pulled straight through the water such that the mean flow is everywhere parallel to the axis of the antenna. The effects of local cross-flow will, however, also be addressed. It should be noted that a local cross-flow (i.e. when the flow direction is misaligned with the axis of the antenna) can occur (i) if the antenna axis is pulled in a different direction than along its axis (’snaking’), *or* (ii) by external flow disturbances such as when the submarine wake creates large three-dimensional flow structures in the vicinity of the antenna. The latter can thus occur even if the antenna is pulled perfectly straight behind the submarine.

2.1 Introductory comments

Before we proceed, some introductory remarks are made that essentially summarizes much of what is going to be discussed later in this report, as well as providing a short summary of selected publications.

2.1.1 Short summary of previous studies

The field of boundary layer turbulence with focus on noise/sound generation constitutes a topic associated with extensive research activities. Axisymmetric boundary layer turbulence has been in particular focus during the last decade or so. The results of these studies are relevant for understanding the impact of flow noise on hull mounted or towed sensor systems. We will give a brief presentation of some of the work that has been done. The presentation is not comprehensive; within the limited time frame of our study only a few papers in the field are referred to.

The topic “Pressure fluctuations beneath turbulent boundary layers” was addressed in 1975 by Willmarth [30]. The motivation for this study was to improve the understanding of the structure of turbulence along with practical aspects like production of noise caused by boundary layer on an aircraft fuselage, and noise caused by the flow over a sonar transducer mounted on ships or submarines. Planar boundary layers were considered in this work. In 1976, Willmarth et al. [31] extended the study to include axisymmetric turbulent boundary layers on cylinders.

In 1980, Panton et al. [22] studied “Low frequency fluctuations in axisymmetric turbulent boundary layers”. In this paper wall pressure fluctuations beneath a turbulent boundary layer were measured on the fuselage of a sailplane. It was found that in the outer portion of the boundary layer, irrotational motions were more highly correlated with the wall pressure than vortical motion. Mean and fluctuating velocities of a turbulent boundary layer on a cylinder were later studied experimentally by Lueptow et al. [16], [17]. They found that Reynolds stress drops off much more quickly with distance from the wall on a cylinder than for a flat plane. The reason is that the peak of turbulent shear stress occurs further away from the wall where the local gradient of axial mean velocity is considerable smaller. As a result, the production of turbulence (in a statistical sense) is lower than in a planar boundary layer.

The flow noise inside a cylinder can be relatively stronger than the noise beneath a flat plate produced by the same fluid due to the fact that as the axial boundary layer is thick compared to the diameter of the cylinder, there may be a larger degree of azimuthal coherence of the flow which inherently amplifies the noise levels. Afzal and Narasimha [1] did an asymptotic analysis of thick axisymmetric boundary layers around circular cylinders; they found that it effectively can be treated as planar boundary layers only if the boundary layer thickness is less or equal the diameter of the cylinder.

A number of numerical studies were carried out by Neves et al. [19] and [20]. They found that convex transverse curvature effects in wall-bounded turbulent flows are significant if the boundary-layer thickness is large compared to the radius of curvature, confirming the theoretical findings of Afzal and Narasimha [1]. As the curvature increases (or the diameter decreases), the surface friction forces per unit area increase; the slope of the logarithmic region decreases; and the turbulence intensities are reduced. Another notable effect of increased curvature was that regions of strong normal vorticity develops close to the wall. Very recently, Joongnyon et al. [13] studied the relationship between wall pressure fluctuations and coherent structures in a turbulent boundary layer. This is also a topic of an ongoing effort in FFI Project 820.

Lueptow, Snarski, and others have in recent papers [2], [18], [26] considered axisymmetric turbulent boundary layers on a cylinder. The goal has been to deduce the effect of transverse curvature on the fluctuating pressure of boundary layer turbulence; all with the underlying motivation to increase the knowledge of flow noise generation. A remarkable finding was that high frequency disturbances observed very close to the wall nearly coincided with the characteristic frequency deduced from the average duration of bursting events. Bursting events is a phenomena that occurs within turbulent boundary layers and these events are believed to contribute significantly to the generation of turbulence. The bursting process provides the two characteristic time scales responsible for the bimodal distribution of energy near the wall. A strong relationship between wall pressure and streamwise velocity as well as between wall shear stress and streamwise velocity was uncovered. The relationship between wall shear stress and wall pressure is on the other hand quite weak. Spanwise coherent structures within the boundary layer are weak and concentrated in a frequency band that is substantially lower than the most energetic frequency band of the

wall pressure spectrum. The bursting frequency thus appears to play a central role in the generation of wall pressure fluctuations, and consequently also flow noise.

Numerical simulations and experiments of axisymmetric (towed and self-propelled) wakes have been carried out by several authors, [5], [11], [12]. They find time scales of hours/days. A consequence is that the length of the wake will extend several kilometers behind the submarine. If the wake is in a stratified environment, some of the energy is radiated away as internal gravity waves, and the wake resolves faster. The effect of stratification will not be elaborated on in this study, although it has a significant impact on the general physical picture.

2.1.2 The array towed in smooth water

A natural starting point of this study is to look at what happens when the array is pulled straight along its own axis through smooth (quiescent) water. This is the case where the flow noise is at a *minimum* level. Even at speeds of $1-2$ m/s the flow that surrounds the array is fully turbulent. We show later that the flow noise generated in this case is higher than Sea State one (SS1) over a broad frequency range. If the array is pulled such that a cross-flow component occurs, the strength of the turbulence intensity is increased on the 'windward' side, whereas it is somewhat decreased on the 'leeward' side. The dominating frequency ranges is also altered, making the physical picture very complicated. By making axially oriented riblets on the surface, the turbulence levels can be somewhat reduced. The same will happen if the antenna is surrounded by a thin layer of polymers that essentially reduce the turbulence levels by interfering with the turbulence generation mechanisms (i.e. lower the bursting frequency). As argued later these 'countermeasures' only result in a minor reduction of the turbulence intensity in thick axisymmetric boundary layers, whereas they work rather efficiently in planar boundary layers.

2.1.3 The array towed in a turbulent wake

We will assume that external (turbulence) disturbaces only are created by the wake itself - effects of ocean currents and such are neglected. The effects of towing the array through a turbulent flow field, as inside the submarine wake, will not only result in increased levels of flow noise as compared to when it is pulled through smooth water, but a significant alteration of the pressure spectrum will also occur. There are two major effects to be addressed: Firstly, the instantaneous large-scale flow field of the wake will have the potential to create a mean cross-flow component relative to the axial velocity, especially in the forward part of the antenna. A significantly more complicated situation then arises [7], [8], [9]. Secondly, the fluctuating portion of the wake flow field has the potential to increase the bursting frequency within the antenna boundary layer, and thus significantly enhance the level flow noise.

It is possible, to a certain extent at least, to quantify the spatial and temporal scales of a self-propelled wake. Simulations and experiments ([5], [11], and [12]) indicate that the

diameter of a axisymmetric turbulent wake will increase with downstream distance as $x^{1/3}$, or as $x^{1/5}$, depending on if it is momentumless or not. We will estimate the diameter and evolution of the wake in a subsequent section.

From measurements and numerical simulations it is possible to estimate the intensity of the turbulence, i.e. the magnitude of pressure and velocity fluctuations in the fluid. A basic problem from an acoustical point-of-view is the difficulty of separating the sound originating from flow noise and that from a remote and perhaps also a weak source. We believe that advanced signal processing algorithms based on insights of turbulence physics will help us separating these two 'components' and thus enhancing the performance of the sonar array.

2.1.4 What is going on inside the array?

Before we proceed with the analysis of the fluid dynamical contribution on the surface of the antenna, let us briefly consider what happens inside the antenna by making use of the recent work reported by Dowling [4], and references therein.

The hydrophones of an acoustic array are located close to the core. The pressure signal at the surface of the antenna is propagated from the surface into the core. The hose and the internal material must be able to support waves; the possible wave modes are elastic p and s modes. The information propagates through an elastic outer hose and toward the core where the hydrophones are located. The pressure signal that reaches the hydrophones is necessarily distorted as compared to the pressure signal at the surface of the array.

The core of towed arrays can be made out of several materials, each with different properties. This acts as a hardware filter reducing the high frequency part of the transmitted fluctuations (be it fluctuations associated with flow noise or fluctuations associated with a remote source). The most common materials are liquid, visco-elastic materials, and "open celled foam". The latter is especially efficient to reduce the amplitudes of the varicose waves (or 'bulge waves') which are 'elastic' longitudinal waves propagating axially along the array; this is a result of the elasticity of the outer hose and the inner material. The "open celled foam" acts a shock absorber limiting the amplitudes of the bulge waves. The bulge wave speed of the hose c_b depends on material parameters. Without the hose, and in the case of a visco-elastic core the phase speed becomes $c_l = \sqrt{E_l/\rho_l}$, where E_l is the elasticity module of the core and ρ_l is the density of the core. Since c_b and c_l are different, the resulting bulge wave speed for the combined waves is a combination of the two. Bulge waves are triggered by the external turbulent flow field leading to pressure resonances at certain frequencies. This implies a peak in the array transfer function that significantly contributes to the 'flow noise' level, i.e. the pressure resonance is thus another type of unwanted 'flow noise'.

Olset [21] has discussed methods for adaptive noise cancellations. The object of his work was to apply filters to seismic streamers, in order to reduce effects of waves propagating axially along the elastic outer hull. The signal from accelerometers attached to the streamer

ends was used as input to adaptive filter functions. The phase velocity of the streamer waves was typically 40 m/s, and the waves are probably dispersive. Most of the power of the noise is at frequencies below 100 Hz. The sampling rate of the system was, on the other hand, 500 Hz which is an upper frequency limit for most seismic streamers. This is somewhat low in order to draw any firm conclusions. The antenna was towed at 5 knots in a lake with noise below Sea State Zero (SS0). The noise is thus a combination of antenna-waves and flow noise; the latter is, however, not considered in the thesis. The conclusions was that the adaptive filters only have a marginal effect above 50 Hz.

A natural question at this point is if the flow noise level be suppressed by altering the dynamics of the turbulent boundary layer? Dowling [4] compares a flat plate (planar) and an axisymmetric turbulent boundary layer on a cylinder. She demonstrated that the resulting pressure signal at hydrophone location has two contributions: (i) from the surface pressure that is accessed through the fluctuating Reynolds stresses within the boundary layer, and (ii) from the fluctuating viscous shear stresses at the surface, cf. equations (2.1) - (2.2). This follows from directly from first principals, cf. Lighthill's theory of sound generation [14], [15].

Dowling also showed that in the cylindrical case (valid for the LOFAR system), the Reynolds stresses in the boundary layer dominate the contribution when evaluating the pressure in the inner part of the array. This indicates that riblets or adding polymers might be of secondary importance for the cylindrical case.

2.1.5 A brief on Lighthill's theory

Turbulence excites acoustical noise. This is a fact. A well-known example is the acoustical noise from a jet engine. The fundamentals of the theory of flow noise was developed by Lighthill see [14], or [15] and references therein. Increased knowledge about flow noise has contributed significantly to the revolution in the design of 'quiet' jet engines.

At the outer boundary of a hydrophone array there is a certain pressure signal which is a superposition of acoustic components, dynamic components caused by turbulence, and hydrostatic components. Ideally, we want high sensitivity to the first of these and wish to avoid the latter two. Following Lighthill's theory, the equation expressing the sound generated by the nonlinear fluid dynamical terms as a source can be written as:

$$\left(c^2\nabla^2 - \frac{\partial^2}{\partial t^2}\right)\rho = -\frac{\partial^2 T_{ij}}{\partial x_i \partial x_j}. \tag{2.1}$$

This follows from the compressible Euler equations, neglecting viscosity in this case (it should be noted that the viscosity can be retained by directly considering the Navier-Stokes equations). The nonlinear source terms in (2.1) are given by the tensor:

$$T_{ij} = \rho v_i v_j + [(p - p_0) - c^2(\rho - \rho_0)]\delta_{ij}. \tag{2.2}$$

For simplicity the viscous terms are neglected, see Dowling [4] for details. Here, v_i denotes the instantanous velocity in the x_i direction whereas $\rho v_i v_j$ is the Reynolds stress tensor. The last term, $[(p - p_0) - c^2(\rho - \rho_0)]$, is the non-linear deviation of sound which can be neglected here. The expression (2.2) can be generalized by adding the viscous stress tensor. These expressions, with appropriate boundary conditions, are formally valid when deriving the acoustic field acting on the hydrophones.

The wave propagation inside the hose has then to be taken into consideration. According to Lighthill's formulation there are two terms responsible for the pressure at the array boundary: The Reynolds stress which maximum contribution comes from a layer close to the array boundary, and the contribution from viscous stress. There is a global coupling between the stresses and the flow noise pressure fluctuations. According to Lighthill's theory, the noise generated by turbulence behaves as quadrupole radiation, i.e. it drops off very fast away form the source $1/r^4$. The consequence is that flow noise is difficult to detect for a remote observer *but* it is not necessarily weak at the surface of the array very close to the 'source' where the Reynolds-stresses peak. Another important result that follows from Ligthill's theory is that the excited sound intensity varies with the speed of the free stream as U^8, which constitutes a dramatic increase with increased speed! Experiments, see [28] show that the flow noise is increaseing with speed as U^6, close to what is predicted by Lighthill's theory.

One should have this in mind in cases where towed arrays or hull-mounted sensors are operated at relative high speeds.

2.2 Fluid properties, design parameters and sound pressure levels

The dimensions used to make qualitative estimates are choosen to represent a typical sonar array configuration; the main findings in this study, however, do not significantly depend on small variations of these geometrical and physical properties:

The fluid properties used throughout this report is that of water at reference temperature $T_{ref} = 5^o$ C:

- Density $\rho = 1000\ \mathrm{kg/m^3}$,
- Kinematic viscosity $\nu \equiv \mu/\rho = 1.519 \times 10^{-6}\ \mathrm{m^2/s}$,

and the dimensions of the towed sonar array:

- Diameter $a = 0.05$ m,
- $L_{antenna} = 350$ m,
- $L_{towing\ cable} = 150$ m.

The background noise level, defined by Sea State One (SS1) is approximately given by the following function of frequency f in Hz:

$$\mathrm{SS1}[f] = 103 - 17\log(f)\,. \tag{2.3}$$

It gives about the right noise level at $f < 50$ Hz, and $f > 10^3$ Hz but it is about 10 dB too high around 200 Hz where the ambient noise level is strongly dependent on ship traffic. We assume light shipping here. Our finding of flow noise levels, however, are compared directly with expression (2.3) without invoking any corrections. The subsequent comparisons are thus conservative in the sense that the background noise level appears higher than light shipping noise in the intermediate frequency regime.

The dynamics of the fluid flow itself creates wall pressure fluctuations, p, that necessarily will be interpreted as 'sound' by the acoustical sensors; the common way to define the sound level in this context is through the so-called 'sound-pressure level'. The relation between pressure fluctuations and sound pressure level (SPL) is given by:

$$\mathrm{SPL}[dB] = 20 \times \log(\frac{p}{p_{ref}}) \tag{2.4}$$

where the reference pressure level $p_{ref} = 1\ \mu$Pa is the commonly used value in underwater acoustics (the corresponding value in air is $p^{air}_{ref} = 20\ \mu$Pa in air). The sound pressure level throughout this report is given in dB relative the reference pressure at 1 meter (e.g. 50 dB re 1 μPa @ 1 m).

2.3 Hydrostatical contribution - structural vibrations

The change of static pressure caused by a vertical displacement (Δh) of the antenna is given by

$$\Delta p(\mathbf{x}, t) = \rho g \Delta h(\mathbf{x}, t). \tag{2.5}$$

The relation to the SPL (in water) is thus

$$\mathrm{SPL}[dB] = 20\log(\Delta h(\mathbf{x}, t)10^{10}) = 20\left[10 + \log(\Delta h(\mathbf{x}, t)\right]. \tag{2.6}$$

Although the antenna mainly would experience low frequency structural vibrations, the necessary amplitude to create significant sound pressure levels is so small that one might need to worry about 'vibrationally' induced flow noise also in the moderate/high frequency regime. This particular effect is believed to be a major source of flow noise that cause problems for seismic streamers technology, cf. e.g. [7]. For example, if $\Delta h = 0.1$ mm then $\mathrm{SPL} = 120$ dB!

2.4 Dynamical contribution - the antenna boundary layer

The pressure fluctuations at the wall beneath a turbulent boundary layer are the result of an integral, or nonlocal, effect of velocity fluctuations. The nonlocality of the pressure stems

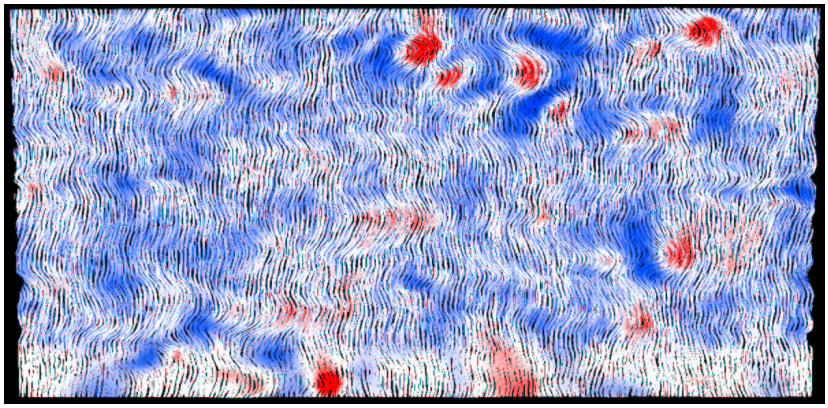

Figure 2.1: Instantaneous vorticity field lines on the wall, colored by the magnitude of the wall pressure fluctuations (red = high, blue = low) in a plane turbulent channel flow. The flow is from left to right. Note that each maxima seems to be accompanied by a pressure minima. Direct numerical simulations conducted in FF project 820.

from the fact that it is goverend by a Poisson equation which can be obtained by taking the divergence of the fluctuating Navier-Stokes equations. For convenience, the planar case is only considered here and the result reads

$$\nabla^2 p = -\left(2\rho \frac{\partial U_i}{\partial x_j}\frac{\partial u_j}{\partial x_i} + \rho \frac{\partial^2}{\partial x_i \partial x_j}\left(u_i u_j - < u_i u_j >\right)\right) \tag{2.7}$$

where p is the fluctuating pressure field. An interesting observation is that the fluctuating pressure field depends not only on the fluctuating velocity field, but also on the *mean* flow field U_i. This equation is elliptical and the solution is therefore *nonlocal*; the wall pressure field depends on the *entire* flow field; *a pressure fluctuation on the wall is therefore not only affected by the near-wall flow field but also on the dynamics of the remote flow field.* Different regions of the flow contributes differently to the generation of wall-pressure fluctuations. As a consequence, external disturbances such as the submarine wake will potentially have significant impact on the generation of wall-pressure fluctuations, and thus also on the generation of flow noise.

The complexity of the turbulent near-wall flow is visualized in figures 2.1 and 2.2. These display the instantaneous wall pressure and vortex structures in a channel flow computation, respectively. These simulations have been conducted in FFI Project 820 'Numerical Simulation of Turbulence and Flow Noise'. There is a complex interplay between the wall pressure fluctuations and the structures within the boundary layer. Such numerical simulations (which solves the time dependent and three-dimensional Navier-Stokes equations) enable us to scrutinize the dynamics of turbulent flow in much greater detail than any experimental measurements ever could provide.

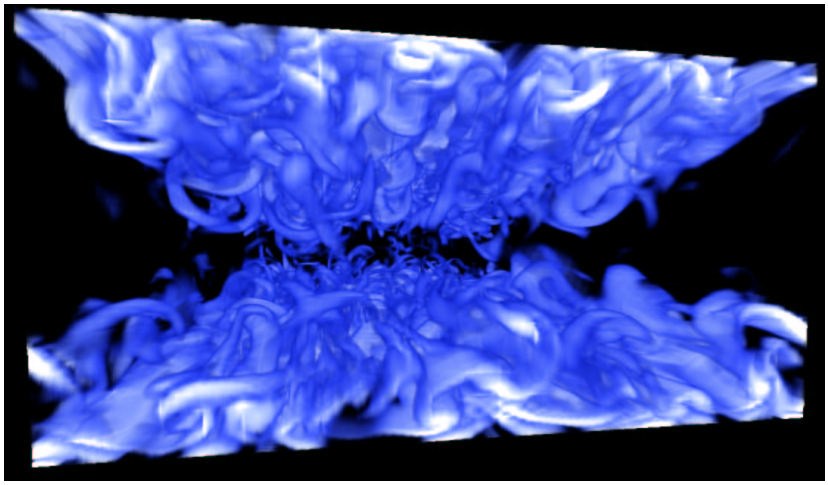

Figure 2.2: Volume rendering of the fluctuating enstrophy field between the two walls in a plane turbulent channel flow. The flow is directed into the paper. Direct numerical simulations conducted in FFI Project 820.

2.4.1 Basic fluid dynamical properties

The discussion of axisymmetric boundary layers usually focuses on how the presence of transverse curvature affects the flows properties and structure with reference to the more well-understood planar ('flat plate') boundary layer. The introduction of an additional length scale (i.e. the cylinder diameter) makes the axisymmetric case more complex.

Consider an antenna with diameter a that is pulled through water in its axial direction with constant velocity U_∞. The surrounding water is assumed to be at rest. The relative motion between the antenna and the water creates a boundary layer with thickness δ due to the no-slip condition on the antenna surface, see figure 2.3. This gives rise to frictional forces which are represented by the so-called friction velocity (u_τ $[m/s]$) defined as

$$u_\tau \equiv \sqrt{\tau_{wall}/\rho} \tag{2.8}$$

where the local wall shear stress $\tau_{wall} = \mu(\partial U/\partial r)_{r=a/2}$. An axisymmetric *mean*[1] flow field can be assumed as long as the antenna is perfectly aligned with its axial direction; i.e. when there are no cross-flow components. The axisymmetric condition is mathematically expressed as $\vec{U} = \{U_x(\vec{x}), U_r(\vec{x}), U_\theta(\vec{x})\} = \{U_x(x,r), U_r(x,r), 0\}$.

Sufficiently far downstream (i.e. at $x/\delta \gg 1$) there are three global length scales that describes this problem

- Viscous length scale; $L_v \equiv \nu/u_\tau$,

[1]The instantaneous velocity components $\tilde{u}_i(\vec{x},t)$ can be decomposed, without loss of generality, into a mean $U_i(\vec{x},t)$ and fluctuating $u_i(\vec{x},t)$ parts; $\tilde{u}_i = U_i + u_i$ where $U_i(\vec{x},t) =< \tilde{u}_i(\vec{x},t) >$ and $u_i(\vec{x},t) = \tilde{u}_i(\vec{x},t) - < \tilde{u}_i(\vec{x},t) >$ where $< .. >$ denotes the ensemble average.

- Cylinder diameter; a,
- Boundary layer thickness; δ,

or more conveniently, three nondimensional parameters associated with these length scales;

- Viscous length scale; $a^+ \equiv a/L_v = au_\tau/\nu$ or $r^+ \equiv r/L_v = ru_\tau/\nu$ $(r \geq a/2)$,
- Cylinder diameter; δ/a, and
- Boundary layer thickness; r/δ.

There are two non-dimensional parameters that involve the viscous length scale; a^+ and r^+. The latter is the 'standard' planar boundary layer parameter whereas the former is particular in the axisymmetric case. $a+$ is only of significance if the boundary layer thickness exceeds the diameter of the cylinder, i.e. at large δ/a. This is because the transverse curvature effect only dominates if $\delta/a \gg 1$. Then, as $a+ \rightarrow O(1)$ the diameter of the cylinder is comparable to the smallest turbulence length scales; a diameter so small that turbulence cannot be sustained on the surface of the cylinder simply because the dynamical structures of the flow do not get sufficient space to exist.

The planar boundary layer is formally recovered in the limit $\delta/a \rightarrow 0$ but the differences between the planar and the axisymmetric boundary layers only becomes significant in practice when $\delta/a > 1$, i.e. when the boundary layer thickness becomes greater than the cylinder diameter as mentioned in section 2.1.1. A simplified picture of this fundamental difference is that the constraining effect of the wall on the large-scale energy containing structures[2] in the boundary layer is significantly weakened. The terminology 'constraining' alludes to the blocking effect of an impermeable solid surface on the flow structures that impinge on the wall. As $\delta/a > 1$, the coherence of the large scale boundary layer structures increases in the circumferential direction which locally intensifies the flow in the near-wall region, and thus also pressure fluctuations. Although this region is *very* thin, $L_\nu \sim 10^{-5}\ m$, it constitutes a crucial portion of the boundary layer where the dynamics of the turbulence are of utmost importance. It is for instance the pressure and velocity fluctuations within this very thin layer that indirectly gives rise to flow noise. It should be recalled the local fluctuations are inherently dependent on the dynamics of the *entire* flow surrounding the antenna. The latter fact is important when it comes to assess the effects of a superimposed wake flow.

Figure 2.4 displays a schematic summary of available experimental data (prior to 2000) on axisymmetric boundary layers reported by Heenan and Morrison [7]. In particular, it depicts a summary of the variation of the boundary layer thickness δ/a with Reynolds number based on the cylinder diameter $Re_a \equiv au_\tau/\nu$ and downstream distance x/a. The general trend is that $\delta/a = \delta/a(Re_a, x/a)$ increases with decreased Re_a and increased downstream distance x/a. Heenan and Morrison also reports the variation of $a^+ = u_\tau a/\nu$

[2] present in the outer portion of the boundary layer; $r \sim \delta + a/2$.

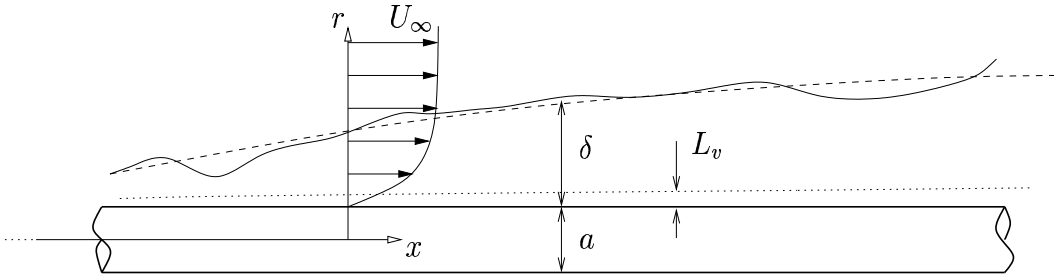

Figure 2.3: Schematic of the flow field viewed in the reference frame of the antenna.

with Re_a and x/a. From these data the characteristic parameters for the present configuration can be obtained:

- $1000 < a^+ < 2000 \Rightarrow \underline{\mathbf{0.03} < \mathbf{u}_\tau[\mathrm{m/s}] < \mathbf{0.06}}$,
- $2 < \delta/a < 5 \Rightarrow \underline{\mathbf{0.15} < \delta[\mathrm{m}] < \mathbf{0.30}}$,
- $5 \times 10^{-5} > L_\nu[\mathrm{m}] > 2.5 \times 10^{-5}$.

The diameter of the turbulent boundary layer ($2\delta + a$) that surrounds the antenna thus varies from approximately 0.3 m at the front to 0.6 m at the far end of the antenna. The boundary layer growth is somewhat slower than in the planar case in which the boundary layer thickness[3] would be expected to grow from $\delta \approx 0.4$ to $\delta \approx 1.4$ m. As the ratio δ/a increases the impact of the antenna surface diminish and the flow resembles that of an axisymmetric wake with a point vortex rather than a fully developed boundary layer.

Figures 2.5 - 2.6 display instantaneous smoke visualization of an axi-symmetric boundary layer conducted at Imperial College at two different Re_a. The boundary layer thickness is approximately 1.0 - 1.5 times the cylinder diameter at this downstream position. Several characteristic features of turbulent boundary layers can be observed: the strong intermittency in the boundary-layer edge region; large scale structures that are tilted in the streamwise direction; and the increased range of scales at the higher Reynolds number (figure 2.6)[4]. It should be kept in mind, however, that the present case is characterised by a significantly higher Reynolds number than the experiments in figures 2.5 - 2.6 ($Re_a = 30000$ at $U_\infty = 1.0$ m/s).

2.4.2 Is the flow turbulent or laminar, and does it really matter?

In order to answer these questions for the flow surrounding the LOFAR antenna, let us start with some basic fluid dynamical aspects. Initially all fluid flows can be considered laminar. Instabilities inherent to all fluid dynamical processes have, on the other hand, a tendency to

[3] $\delta_{planar} \approx 0.37 \times L^{3/4} \times (\nu/U_\infty)^{1/5}$.

[4] As the Reynolds number increases, and the boundary layer thickness stays approximately the same, the size of the small scale turbulence is decreased. The range of scales is thus increased.

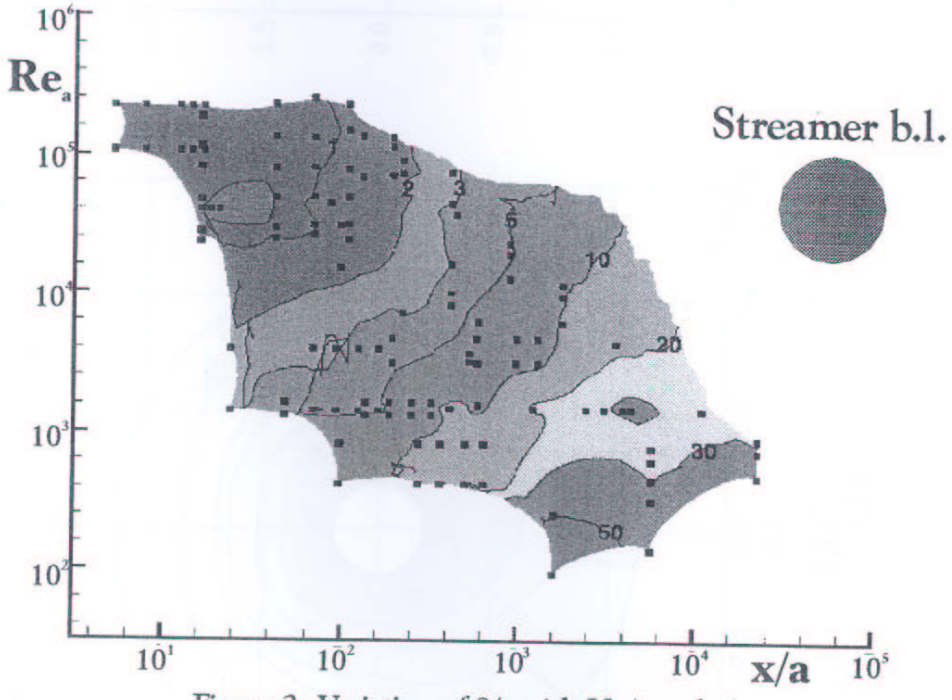

Figure 2: Variation of δ/a with Ua/ν and x/a

Figure 2.4: Variation of δ/a as a function of Re_a and x/a. Figure taken from [7].

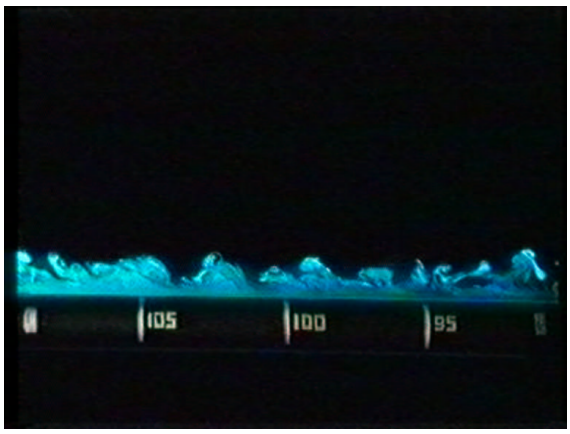

Figure 2.5: Axi-symmetric boundary layer measurements at $Re_a = 3000$ and $\delta/a \sim 1.5$ reported by Heenan and Morrison [7]. Smoke visualization of boundary layer structures. The flow is from right to left.

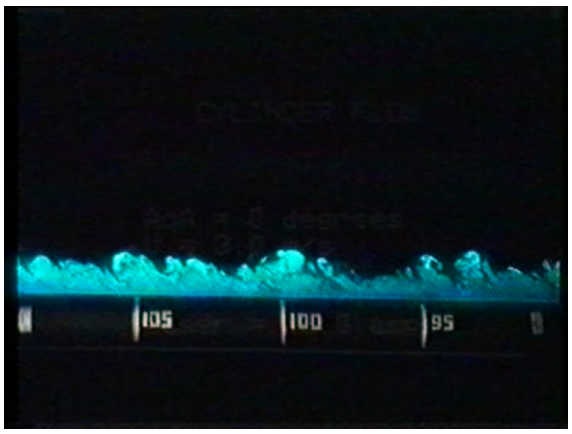

Figure 2.6: Axi-symmetric boundary layer measurements at $Re_a = 6000$ and $\delta/a \sim 1.5$ reported by Heenan and Morrison [7]. Smoke visualization of boundary layer structures. The flow is from right to left.

transform the smoothness associated with laminar flows to a seemingly chaotic and random fluid motion which we refer to as a turbulent state. These instabilities basically comes into play when the inertial force that acts on a fluid element becomes sufficiently large compared to the viscous force. The inertia-to-viscous force ratio defines the so-called Reynolds number (Re):

$$Re = \frac{\text{Inertia force per unit area}}{\text{Viscous force per unit area}} \equiv \frac{\rho V^2}{\mu V/L} = \frac{VL}{\nu} \tag{2.9}$$

where V, L and ν denote the characteristic velocity, characteristic length and kinemtaic viscosity. In a boundary layer $V = U_\infty$ and $L = |x - x_0|$, so $Re_x = Ux/\nu$ if we choose $x_0 = 0$. If we on the other hand consider a cylinder with diameter a in crossflow with velocity U_c, then $V = U_c$ and $L = a$, so $Re_a = U_c a/\nu$. When the Reynolds number becomes large enough, the influence of viscous forces diminish and the flow becomes inherently unstable; i.e. it becomes turbulent.

In virtually *all* practical situations an axisymmetric boundary layer, including the present case, is *fully turbulent* because $x \gg \nu/U_\infty$. Exceptions do exist, however, and these are basically limited to two cases which are presented in table 2.1, either one of them will be sufficient to sustain a laminar flow field. For example, at $U_\infty = 1$ m/s the flow stays laminar roughly a distance $x \approx 0.3$ m downstream the cylinder leading edge; the viscous forces are sufficiently large the first 0.3 meters of the cylinder to prevent flow instabilities to grow and turbulence to develop. This approximation is however not independent of cylinder diameter, but for all practical purposes it is a good approximation; also in the present case.

If, on the other hand the antenna diameter is *really, really* small, the antenna surface would be too small to accomodate the turbulence-generating mechanisms in the boundary layer [10]. Let us estimate how small a diameter that would be necessary to ensure laminar flow conditions in the present case (almost) independent of the downstream distance. It has been established [10] that the turbulence-generating structures are spaced approximately 100 so-called '+-units' in the spanwise direction[5] in planar boundary layer; i.e. $zu_\tau/\nu \approx 100$ where z is the (dimensional) spanwise distance. These structures are essentially two counterrotating streamwsie vortices that thus only exist in pairs. A cylinder with diameter a has an equivalent spanwise extension of $2\pi a$ so the minimum diameter to accomodate two of these turbulence-generating structures is $a_{min} \approx 2 \times 100/2\pi \approx 32$. This is the estimate provided in table 2.1. From the summary of experimental data reported by Heenan and Morrison [7], $u_\tau \sim 0.03$ m/s at $U_\infty = 1$ m/s, so the cylinder diameter need to be smaller than $a = 32\nu/u_\tau \approx 0.0016$ m, i.e. 1.6 millimeter (!) in order for laminar flow to be sustained at $U_\infty = 1$ m/s.

To this end we have only discussed the flow which is more or less aligned with the axial direction of the antenna. The other extreme is a pure cross flow[6]. The relevant Reynolds number in this case is based on the cylinder diameter, i.e. $Re_a = U_c a/\nu$. The critical (or transitional) Reynolds number $Re_a^{critical} \sim 10^4 - 10^5$, see e.g. [3], is about the same as for the axisymmetric case. While the axisymmetric boundary layer can be considered as

[5] perpendicular to the streamwise and wall-normal directions.

[6] The direction of the flow is perpendicular to the axis of the antenna.

(i)	$Re_x \equiv xU_\infty/\nu \leq 2 \times 10^5$	$\Leftrightarrow$	$x \leq 0.3/U_\infty \ (m)$
(ii)	$a^+ = a/L_v < a_0^+ \approx 32$	$\Leftrightarrow$	$a < a_{min} \approx 4.8 \times 10^{-5}/u_\tau \ (m)$

Table 2.1: Rule-of-thumb parameters for laminar flow conditions. It suffices that one of these requirements are met.

turbulent for all practical purposes, the boundary layers associated with the pure crossflow case are in the so-called transitional regime[7]. The effects of cross-flow is further discussed in section 2.6.3.

With the exception of pure crossflow where a laminar boundary layer exerts higher dynamical forces than a turbulent one, the turbulent state totally dominates the flow field surrounding the antenna. The structure and dynamics of the flow have a crucial impact on the generation of acoustical noise, or more correctly the fluctuating pressure field. A turbulent flow field has invitably a greater impact due to the enormous range of scales that exists in high a Reynolds number boundary layer such as this. As will be shown in the subsequent section, it creates a broadband pressure spectrum with significant amplitudes that potentially can exceed that of the far field, or background noise, level.

2.5 Turbulence generated noise

In order to assess the fluid dynamical induced sound pressure levels on the surface of the antenna as a function of frequency we can make good use of existing experimental data. To this end we have adopted the measured pressure power spectrum Φ_p reported by Snarski [24]. The pressure power spectrum is related to the pressure fluctuations and dynamical pressure $q \equiv 1/2 \ \rho U_\infty^2$ through the relationship:

$$\frac{\overline{p^2}}{q^2} = \int_0^\infty \Phi_p df, \tag{2.10}$$

and the root-mean-square pressure fluctuations $p \equiv \sqrt{\overline{p^2}}$. The values of the left hand side of (2.10) has been reported in numerous papers, see e.g. table 2.2.

Figure 2.7 shows a model spectrum based on measurements [24]. It should be noted that no data was available for $f < 57$ Hz; the model has simply been extrapolated for $1 < f < 57$ which makes comparisons in this regime more uncertain than for higher frequencies. From the modeled spectrum we can obtain the functional dependence $p = p(f)$. This is done in the following way: We assume that $\Phi_p = Af^n$, where A is a constant and n varies

[7] a state of neither sustained laminar flow, nor fully developed turbulence

Investigations	Re_a	$\sqrt{\overline{p^2}/q^2} \times 10^3$
Snarski and Lueptow [26]	3644	8.64
Nepomuceno and Lueptow [18]	3216	9.40
Bokde and Lueptow [2]	3300	9.25
Snarski [24]	3640	8.64
Heenan and Morrison [8]	54000	7.80
FFI (Proj. 820)*	–	10.6

*Table 2.2: Experimental results of wall-pressure measurements in axisymmetric boundary layers. The Reynolds number in the present case is $Re_a \approx 3 \times 10^4$ at $U_\infty = 1$ m/s. * The FFI data is from a plane channel simulation (not directly comparable)*

according to figure 2.7;

$$\frac{\overline{p^2}}{q^2} = \int_{f_0}^{f_1} A_1 f^{1/3} df + \int_{f_1}^{f_2} A_2 f^{-1/6} df + \int_{f_2}^{f_3} A_3 f^{-1} df + \int_{f_3}^{f_4} A_4 f^{-2} df + \int_{f_4}^{f_5} A_5 f^{-5} df, \tag{2.11}$$

where $f_0 = 0$, $f_1 = 200$, $f_2 = 600$, $f_3 = 1000$, $f_4 = 2000$ and $f_5 = 6700$.

The constants A_i are not independent since they must obey the following matching constraints in order to retain a continous model spectrum:

$$A_1 f_1^{1/3} = A_2 f_1^{-1/6};\ A_2 f_2^{-1/6} = A_3 f_2^{-1};\ A_3 f_3^{-1} = A_4 f_3^{-2};\ A_4 f_4^{-2} = A_5 f_4^{-5}. \tag{2.12}$$

Any 4 of the constants can now be expressed in terms of the 5th. The result can e.g. be written as

$$\frac{\overline{p^2}}{q^2} = 6.29 \times 10^3 \times A_1. \tag{2.13}$$

The left hand side can be directly taken from the experimental data [24]: With $p/q = 8.64 \times 10^{-3}$ where $q = 1/2\rho U_\infty^2 = 500$ Pa ($U_\infty = 1$ m/s), $A_1 = 1.187 \times 10^{-8}$. The remaining constants then becomes; $A_2 = 1.678 \times 10^{-7}$, $A_3 = 3.465 \times 10^{-5}$, $A_4 = 3.465 \times 10^{-2}$ and $A_5 = 2.777 \times 10^8$.

The fluctuating pressure can now be determined as a function of frequency:

$$p = \sqrt{A_1 f^{1/3}}; \quad 57 \leq f\ (Hz) < 200 \tag{2.14}$$
$$p = \sqrt{A_2 f^{-1/6}}; \quad 200 \leq f\ (Hz) < 600 \tag{2.15}$$
$$p = \sqrt{A_3 f^{-1}}; \quad 600 \leq f\ (Hz) < 1000 \tag{2.16}$$
$$p = \sqrt{A_4 f^{-2}}; \quad 1000 \leq f\ (Hz) < 2000 \tag{2.17}$$
$$p = \sqrt{A_5 f^{-5}}; \quad 2000 \leq f\ (Hz) < 6700. \tag{2.18}$$

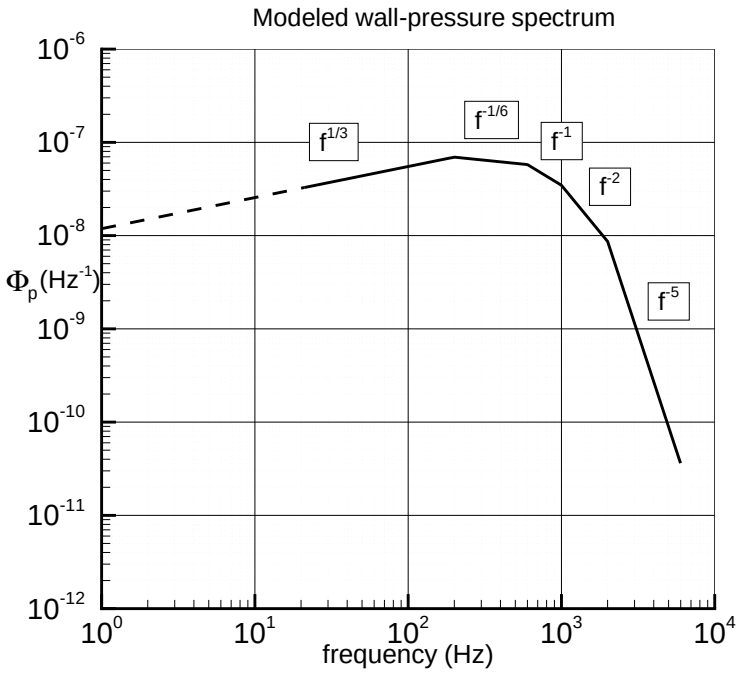

Figure 2.7: Model spectra taken from [24].

The sound pressure level is now readily computed by using equation (2.4). The result is shown in figure 2.8 where also SS1 (2.3) is plotted.

As can be seen from its definition, the fluctuating root-mean-square pressure depends linearly on the dynamic pressure $1/2\ \rho U_\infty^2$. This scaling has significant consequences if the towing velocity is increased; p increases as the square of U_∞. Figure 2.9 display the difference between the SPL and SS1, and the signal-to-noise ratio as a function of freestream velocity, respectively. It should, however, be noted that the effect of increased freestream velocity displayed in figure 2.9 is based on the simplifying assumption that the spectrum preserves its shape, but $\overline{p^2}/q^2$ increases, as the freestream velocity increases. As pointed out by Mjølsnes (private communication), this is of course not entirely true. The displayed results nevertheless give a useful qualitative measure of the effect of increased towing speed since the integral of the spectrum, i.e. the level of $\overline{p^2}/q^2$, is in accordance with existing measurements.

The experimental (and numerical) results displayed in table 2.2 are all virtually based on point measurements of the pressure, e.g. very small diameter microphones ($d \sim 1$ mm). Schewe [23] investigated the effects of varying the microphone diameter on the recorded wall-pressure fluctuations. The main finding was that p/q decreases as the diameter of the microphone increases due to the filtering effect. The data suggests a reduction from $p/q \approx 9 \times 10^{-3}$, for a point measurement (cf. table 2.2), to e.g. $p/q \approx 4 \times 10^{-3}$ for $d \approx 0.05$ m. The qualitative effect of increasing the sensor diameter (from 1 to 50 mm) on the SPL is shown in figure 2.10. The effect is assumed to be independent of frequency for

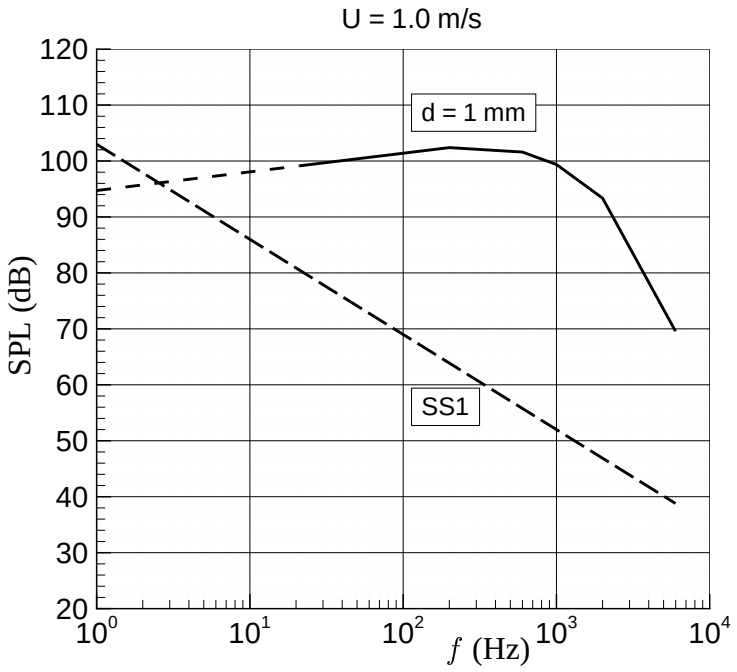

Figure 2.8: Modeled sound pressure level (SPL) and SS1 at $U_\infty = 1$ m/s. The SPL curve is dashed at the lower frequencies because no experimental data was available for $f < 60$ Hz. d is the diameter of the microphone used in the experiments.

simplicity.

2.6 Dynamical contribution - the submarine wake

To this end we have considered the antenna boundary layer in isolation - we have assumed that it could live its life without external disturbances. There are numerous disturbances to account for but the natural starting point is the submarine generated wake; its initial characteristic and its evolution in time. Figure 2.11 displays a submarine generated wake with the characteristic shape. The wake will set up a nonuniform flow field that could be viewed as an outer 'forcing' of the dynamics of the axisymmetric boundary layer discussed in the previous sections; the wall-pressure generating events within the boundary layer (i.e. the sound pressure level) will thus also be affected. Hancock and Bradshaw [6] reported some experimental work on planar boundary layers and isotropic grid turbulence, but unfortunately not with the objective to quantify the effect on the wall-pressure fluctuations. At this point, therefore, it is very difficult to arrive at a quantitative conclusion about the interaction relavant for the LOFAR system. To the knowledge of the authors, as well as Dr. Stephen Snarski at the Naval Undersea Warfare Centre (NUWC), Newport, USA (private communication), the interaction between external disturbances (such as the highly anisotropic turbulent submarine wake) and an axisymmetric boundary layer have not yet

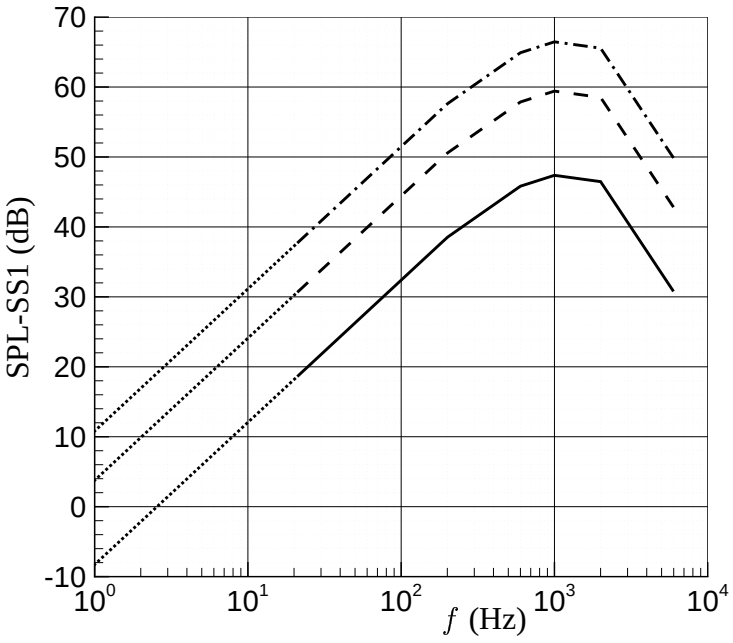

Figure 2.9: The difference between the sound pressure level and sea state one (SPL - SS1) as a function of freestream velocity; $U_\infty = 1,\ 2,\ 3$ m/s, respectively, plotted from bottom to top.

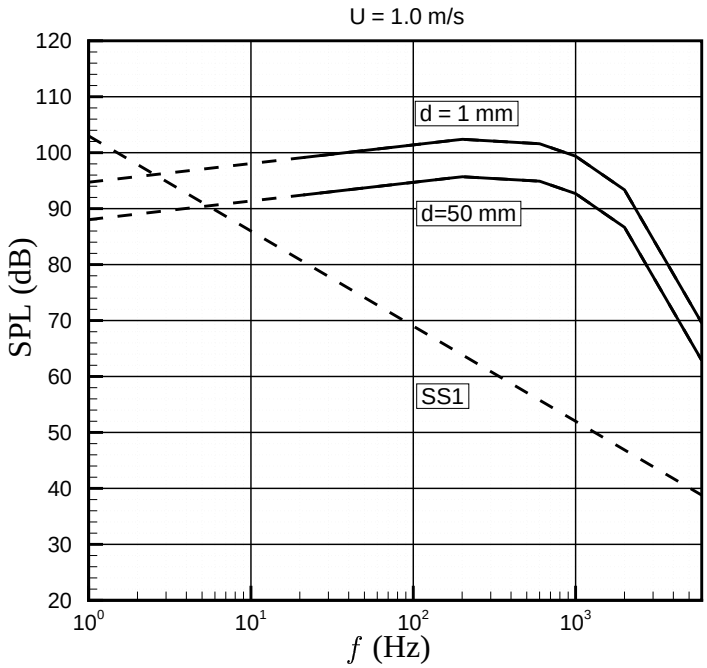

Figure 2.10: Effect of sensor diameter on the sound pressure level at $U_\infty = 1.0$ m/s. The effect is assumed to be independent of frequency for simplicity.

Figure 2.11: The wake behind the French submarine 'Le Triomphant'.

been reported in the literature. Any quantitative conclusion concerning this interaction would need to rely on further studies, but some estimates will be presented in the following sections.

2.6.1 The initial wake

In order to estimate the initial diameter of the submarine wake, we first need to estimate the submarine boundary layer thickness. The boundary layer along the submarine hull is fully turbulent, except perhaps for a small region in the front. The boundary layer is turbulent due to the enormous Reynolds number: $Re_L = U_\infty L/\nu \approx 9.1 \times 10^7$ at the end of the submarine at $U_\infty = 1$ m/s. The thickness of the submarine boundary layer δ grows as a power of downstream distance, x, but decreases with increased towing velocity. Since the transverse curvature of the submarine hull is much greater than the boundary layer thickness it suffices to use the empirical relation valid for planar boundary layers:

$$\delta_{planar} \approx 0.37 \times L_\infty \times Re_L^{-1/5}. \tag{2.19}$$

With $L_\infty \approx 60$ m and $U_\infty = 1$ m/s, this gives $\delta \approx 0.7$ m. The initial wake diameter could thus be estimated as

$$D_{wake}^{x=0} = 2 \times \delta + D_{uvb} \approx 6 \text{ m}$$

where D_{uvb} is the diameter of the submarine at the control surfaces leading edge (say $D_{uvb} \sim 4 - 5$ m).

The initial diameter of the wake, however, is not simply axisymmetric; it is asymmetric mainly because of downstream effects of the submarine sail. The thickness of the initial wake in the horizontal plane will, however, not be altered. In summary, the initial wake will resemble more an ellipse than a circle and have a semi-major diameter of approximately 9 m, and a semi-minor diameter of approximately 6 m. In the subsequent sections we are using the average diameter $D_{avg} = \sqrt{6 \times 9} \approx 7$ m. This is our starting point to estimate the evloution of the wake downstream the submarine. Before we do this, a brief comment about the boundary layer turbulence will be made.

2.6.2 The evolution of the wake

The submarine wake is self-propelled, i.e. it is momentumless. The evolution of the wake is therefore different from 'ordinary' wakes in the literature which usually are not momentumless - they are so-called 'towed' wakes. Experimental results indicates that the latter type grow radially with downstream distance as $x^{1/3}$ whereas momentumless wakes grow at a slow rate: $x^{1/5}$, see e.g. [12]. These estimates inherently assume that the submarine does not maneuver (decelerate/accelerate or change direction) and that there are no effects of density stratification. The wake diameter at a distance x measured from the submarine can thus be estimated from the relation:

$$D_{wake} \approx D_{wake}^{initial} + 2 \times x^{1/5} = 7.0 + 2 \times x^{1/5} \tag{2.20}$$

where $D_{wake}^{initial}$ is the initial wake diameter created by the submarine itself.

The velocity defect[8] of a momentumless wake (neglecting the propeller induced swirl) decays fast downstream the submarine; at a downstream distance $x = 500$ m the velocity defect $U_d \sim 0.015$ m/s (with towing speed $U_\infty = 1$ m/s) which is relatively weak. On the other hand, the turbulence fluctuations have, somewhat surprisingly, a *larger* amplitude than U_d within a downstream range of $100 \leq x \leq 840$ m): $u \sim 1.15 \times U_d \approx 0.02$ m/s, cf. [12]. This is *not* neglegible; the root-mean-square of the turbulent fluctuations *within* the antenna boundary layer at $x \sim 500$ m *peaks* in the streamwise direction at $u \approx 0.09$ m/s, whereas the radial component peaks at $v \approx 0.03$ m/s [16]. Given the inherent nonlocal nature of the pressure (cf. equation 2.7), the external disturbances caused by the submarine wake, even 500 m downstream with $U_\infty = 1$ m/s, are expected to significantly affect the pressure power spectrum and consequently increase the pressure sound levels.

Figures 2.12 -2.15 display vortical structures behind an axisymmetric wake as a function of distance behind the wake-generator (e.g. a submarine) obtained from high performance numerical simulations [5]. The data shown here only corresponds to the so-called 'near-wake' part of the simulation; the entire data simulation covers a downstream distance that corresponds roughly to $x/D \sim 60000$, i.e. 420000 meters behind an Ula submarine! This unique database makes it possible not only to study the wake dynamics but also the interaction with external shear, stratification, and a swirling motion generated by the propeller. It is made available to us through the FFI Project 820 in which we work in close collaboration with scientists at Colorado Research Associates (CoRA) who conducted this enormous simulation.

A notable feature of the results displayed in figures 2.12 -2.15 is the decay time, i.e. the time it takes to for the wake to be dissipated, and the slow growth (these are of course coupled effects). Note that the distance from the self-propelled body has increased from approximately 540 m (figure 2.12) to 4500 m (figure 2.15), whereas the wake diameter only has increased from 14 to 18 m. In fact, experimental results ([27], [29],[12]), report a decay time for wakes in the order of several days (!). Voropayev et al. [29] experimentally discovered that maneuvering submerged self-propelled bodies, in the far-wake regime when stratifiaction is present, may be expected to create very large, slowely moving eddies with a diameter in the order of 1000-2000 meters on the surface which decayed very slowly (several days).

The primary conclusions about the effect of towing the antenna through the wake is that the sound pressure level is amplified through both the wakes local (cross flow) and nonlocal (pressure fluctuations) interaction with the antenna boundary layer. In particaular:

- the wake will influence the local flow condition along the entire antenna,
- the local fluid motion within the wake, on a relatively large scale, will introduce a cross flow component over the antenna, as well as increased correlation lenght scales.

[8] defined as $U_d \equiv \max[U_\infty - U(x,r)]$ where $U(x,r)$ is the axial mean velocity component at a downstream distance x behind the wake generator (i.e. the submarine).

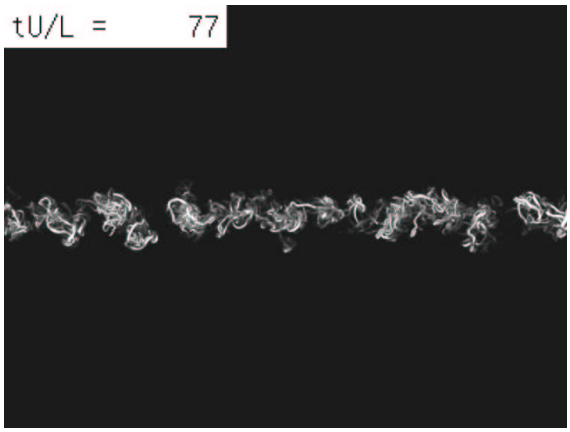

Figure 2.12: Numerical simulations of an axisymmetric wake [5] showing the vortical signature approximately 540 m behind the wake-generator ($U_\infty = 1.0$ m/s). The diameter of the wake at this point in time is approximately $D \approx 14$ m. Fluctuating velocity $u \sim 0.02$ m/s. Note the L in Gourlay et al. [5] notation equals the initial wake diameter, i.e. $L = D_{avg} = 7$ m.

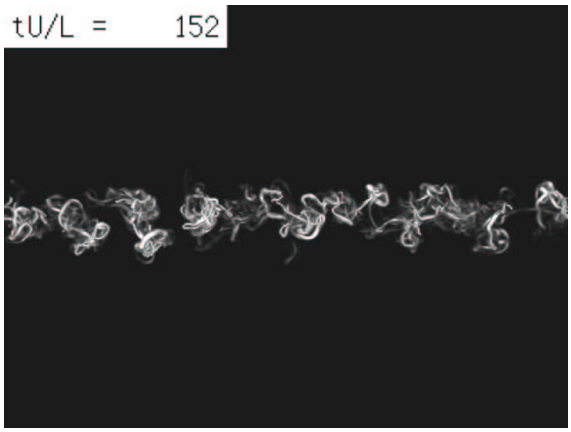

Figure 2.13: For captions see figure 2.12. Downstream distance approximately 1060 m, wake diameter $D \approx 15$ m, and fluctuating velocity $u \sim 0.01$ m/s.

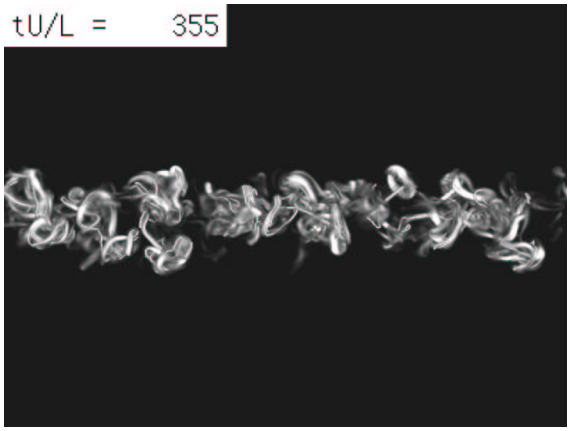

Figure 2.14: For captions see figure 2.12. Downstream distance approximately 2500 m, wake diameter $D \approx 17$ m, and fluctuating velocity $u \sim 0.006$ m/s.

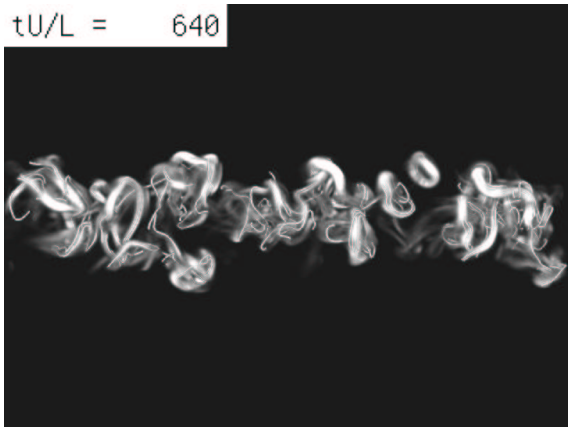

Figure 2.15: For captions see figure 2.12. Downstream distance approximately 4500 m, wake diameter $D \approx 18$ m, and fluctuating velocity $u \sim 0.004$ m/s.

Finally, and perhaps the most disturbing issue with turbulent wakes; the exact evolution of the wake is not only dependent on the diameter of the wake-generator and on the free-stream velocity, it is also dependent on the *three-dimensional geometry* of the wake generator, see e.g. [12]. Put in other words, the shape and growth rate of the wake will vary depending on the geometry of the object that created it, e.g. it will be dependent on shape of the entire submarine. This makes any attempt to quantify the wake behind an Ula-class submarine very difficult, if not impossible. On the other hand, the qualitative estimates provided in this initial study is probably not far from the truth, and there are possiblities to improve these in future studies. No attempts have been made here, however, to characterise the details of the wake flow.

2.6.3 Effects of wake induced cross-flow

The large scale wake field will locally induce cross flow on the antenna. Recent experiments carried out at Imperial College [7] assessed the effects of small cross flow ($0 - 6^{\circ}$) on a transversely curved boundary layer. It is obvious that the situation gets significantly more complicated since the flow ceases to be axisymmetric; the sensors positioned circumferentially on the antenna are affected differently. On the upstream side, the magnitude of the root-mean-square wall pressure fluctuations p increases, and thus also the sound pressure levels, whereas p is somewhat reduced on the leeward side with a shift in frequency. The circumferentially averaged wall pressure is on the other hand slightly reduced.

Bull and Dekkers [3], among others, have made an important observation concerning thick ($\delta/a \gg 1$) axisymmetric boundary layers, which is relavant for towed sonar arrays: large-scale turbulence within the boundary layer itself may well play a significant part in the production of vorticity within the layer. Such cross-flows may produce localized transient features that produce gross changes in the mean velocity distribution even at very small yaw angles. The susceptibility for these episodic events are large within the range $10^4 < Re_a < 10^5$, which thus includes the present configuration ($0.3 < U_{\infty}[\text{m/s}] < 3$).

Recent work by Snarski [25] indicates that it seems to exist four different flow regimes depending on the yaw angle[9]:

1. $0 \leq \alpha < 15$: Axial boundary layer;
2. $15 \leq \alpha < 45$: Attached trailing vortices;
3. $45 \leq \alpha < 60$: Fully separated turbulence;
4. $60 \leq \alpha < 90$: 'Traditional' Strohaul vortex shedding.

The latter regime, (4), consists of strong narrowband energy levels at low frequencies ($f < 10$ Hz) associated with an organised shedding motion. Regime (3), on the other hand,

[9] $\alpha = 0$ corresponds to a perfect alignment between the mean flow and the cylinder axis.

is characterized by a high-level broadband energy indicative of a fully separated turbulent flow with no organised shedding present. The organised vortex shedding reappeard, however, in regime (3). The latter regime seemed to be associated with sheets of attached vortices with narrowband energy peaks at $f < 10$ Hz. Regime (1) is characterised by an entirely broadband spectrum as considered in detail earlier in this report. NUWC currently also undertakes experiments of a curved antenna configuration with the objective to investigate the complex interplay between the antenna boundary layer and a skewed inflow.

3 CONCLUDING REMARKS

We have assessed the impact of turbulence generated pressure-fluctuations *on the outer skin* of a towed sonar array (or hull-mounted sensor) based on available literature. In addition, we have briefly discussed the transfer of waves within the antenna itself. The latter mechanism can conveniently be separated from the former; there is no impact of waves propagating inside the array on the dynamics outside, and on the surface, of the antenna. It has been indicated that, depending on the material properties of the antenna, resonances may occur inside the antenna that strongly, and detramental to the performance, affects the sesnor elements. The main focus of attention in this introductory study, however, has been on the fluid dynamical behaviour. The main findings are briefly summarised in subsequent sections.

3.1 The antenna boundary layer

- The antenna boundary layer is fully turbulent with thickness $0.15 \leq \delta/a[\mathrm{m}] \leq 0.30$ (increasing downstream).
- For yaw angles $\alpha \leq 15$ degrees: broadband energy spectrum with sound pressure levels (SPL) significantly higher than SS1 over a broad frequency range even at $U_\infty = 1$ m/s.
- For yaw angles $\alpha > 15$ degrees: narrowband energy peaks at low frequencies ($f < 10$ Hz) associated with very high SPL. The broadband spectrum at higher frequencies probably prevails with SPL higher than SS1.
- Increasing the sensor area decreases SPL.
- Increased free-stream velocity significantly increases SPL.

3.2 The submarine wake

- The fluctuating flow field generated inside the wake is sufficiently strong to affect the antenna in its entire length.

- The impact on the wall-pressure fluctuations cannot be established at this point. There is, however, no reason not to expect a significant increase of SPL since high levels of fluctuations prevail along the entire antenna.
- Grows radially downstream very slowely from approximately $D_{\text{wake}}^{x=150} \approx 12$ to $D_{\text{wake}}^{x=500} \approx 14$ m.
- It triggers a relatively weak local mean cross-flows which have a tendency to create low frequency energy peaks.

4 RECOMMENDATIONS FOR FUTURE STUDIES

The results of this study show that turbulence generated flow noise on towed, or hull-mounted, sensors are significant. It therefore seems necessary to further address this problem in order to understand how flow noise affects these systems which necessarily has an adverse impact on the performance. The conducted literature survey has revealed lack of important knowledge in this field, especially related to axi-symmetric boundary layers, and its interaction with external disturbances (such as a wake). Not even the physical picture of how the wall-pressure fluctuations beneath a turbulent boundary layer are created and maintained is not yet complete. An answer to this would enable an evaluation that would establish if passive or active flow control measures could be a viable approach to reduce the problem. These approaches also include adaptive signal processing, and turbulence theory will probably provide us with means to suppress the effect of flow noise on towed acoustical arrays and hull-mounted sensors systems.

The interaction between the outer turbulent field and the antenna will induce a pressure signal that can be propagated into the core of the antenna. Presently available computing power is insufficient to simulate compressible and fully developed turbulence in the ocean. It is possible then to perform incompressible simulations. To quantify the sound excited by the turbulence, Lighthill's formulation is used as a post processing step.

The response of the turbulent fluctuations inside the antenna is expected to be different for the incompressible pressure fluctuations of the turbulent boundary layer (they are evanescent?) and the acoustical pressure fluctuations excited by the turbulent boundary layer. To uncover the differences and then the resulting noise reaching the hydrophones inside the antenna it is necessary to do simulations of: (i) A fully developed cylindrical incompressible turbulent boundary layer, (ii) the resulting flow noise accessed through Lighthill's formulation, and (iii) the propagation of the resulting field in the interior of the antenna. The signal is propagated through the elastic hose via proper boundary conditions. When the interior fields are available, the effect of various signal processing algorithms can be tested out.

5 ACKNOWLEDGEMENT

We would like to thank Svein Mjølsnes (FLO/M) and Tor Knudsen (FFI) for useful and constructive comments that helped improve the final version of this report.

References

[1] N. Afzal and R. Narasimha. Asymptotic analysis of thick axi-symmetric turbulent boundary layers. *AIAA J.*, 23:963–965, 1985.

[2] A. L. W. Bokde and R. M. Lueptow. Span wise structure of wall pressure on a cylinder in axial flow. *Phys. Fluids*, 11(1):151–161, 1999.

[3] M. K. Bull and W. A. Dekkers. Vortex shedding from long slender cylinders in near-axial flow. *Phys. Fluids*, 5(12):3296–3298, December 1993.

[4] A. P. Dowling. Underwater flow noise. *Theoret. Comput. Fluid Dynamics*, 10:135–153, 1998.

[5] M. J. Gourlay, S. C. Arendt, D. C. Fritts, and J. Werne. Numerical modeling of initially turbulent wakes with net momentum. *Phys. Fluids*, 13:3783, 2001.

[6] P. E. Hancock and P. Bradshaw. Turbulence structure of a boundary layer beneath a turbulent free stream. *J. Fluid Mech*, 205:45–76, 1989.

[7] A. F. Heenan and J. F. Morrison. Velocity- and pressure-field measurements in the turbulent boundary layer surrounding a slender cylinder in axial and near-axial flow. Technical report, Department of Aeronautics Turbulence & Mixing Group, May 1999.

[8] A. F. Heenan and J. F. Morrison. Turbulent boundary layers on axially inclined cylinders. Part 1. Surface-pressure/velocity correlations. *Experiments in Fluids*, 32:547–557, 2002.

[9] A. F. Heenan and J. F. Morrison. Turbulent boundary layers on axially inclined cylinders. Part II. Circumferentially averaged wall-pressure wavenumber-frequency spectra. *Experiments in Fluids*, 32:616–623, 2002.

[10] J. Jimenez and P. Moin. The minimal flow unit in near-wall turbulence. *J. Fluid Mech.*, 225:213–240, 1994.

[11] P. B. V. Johannson. *The axisymmetric turbulent wake*. PhD thesis, Chalmers University of Technology, Gothenburg, Sweden, 2002.

[12] P. B. V. Johansson, W. K. George, and M. J. Gourlay. Equilibrium similarity, effects of initial conditions and local Reynolds number on the symmetric wake. *Phys. Fluids*, 15(3):603–617, 2003.

[13] K. Joongnyon, C. Jung-II, and J. S. Hyung. Relationship between wall pressure fluctuations and streamwise vortices in a turbulent bondary layer. *Phys. Fluids*, 14(2):898–901, February 2002.

[14] M. J. Lighthill. On sound generated aerodynamically, part I: General theory. *Proc. Roy. Soc. London Ser. A*, 211:564–587, 1952.

[15] Sir James Lighthill. *Waves in fluids*. Cambridge University Press, 1978. ISBN 0 521 29233 6.

[16] R. M. Lueptow and J. H. Haritonidis. The structure of the turbulent boundary layer on a cylinder in axial flow. *Phys. Fluids*, 30(10):2993–3005, 1987.

[17] R. M. Lueptow, P. L. Leehey, and T. Stellinger. The thick, turbulent boundary layer on a cylinder: Mean and fluctuating velocities. *Phys. Fluids*, 28(12):3495–3505, 1985.

[18] H. G. Nepomuceno and R. M. Lueptow. Pressure and shear stress measurements at the wall in a turbulent boundary layer on a cylinder. *Phys. Fluids*, 9(9):2732–2739, 1997.

[19] J. C. Neves and P. Moin. Effects of convex transverse curvature on wall-bounded turbulence. Part2. The pressure fluctuations. *J. Fluid Mech.*, 272:383–406, 1994.

[20] J. C. Neves, P. Moin, and R. D. Moser. Effects of convex transverse curvature on wall-bounded turbulence. Part1. The velocity and vorticity. *J. Fluid Mech.*, 272:349–381, 1994.

[21] K. Olset. Noise cancellations on seismic streamers. Master's thesis, Norwegian Technical University (NTNU), 1994. Adaptive noise cancellation.

[22] R. L. Panton, A. L. Goldman, R. L. Lowery, and M. M. Reischman. Low-frequency pressure fluctuations in axisymmetric turbulent boundary layers. *J. Fluid. Mech*, 97(2):299–319, 1980.

[23] G. Schewe. On the structure and resolution of wall-pressure fluctuations associated with boundary layer flows. *J. Fluid. Mech*, 134:311–328, 1983.

[24] S. R. Snarski. Relation between the fluctuating wall pressure and the turbulent structure of a boundary layer on a cylinder in axial flow. Technical report, Naval Undersea Warfare Center Detachment, Submarine Sonar Department, Division Newport, 1993. NUWC-NPT Technical Report 10223.

[25] S. R. Snarski. Flow over yawed circular cylinders: Wall pressure spectra and flow regimes (to appear). *Phys. Fluids*, 2004.

[26] S. R. Snarski and R. M. Lueptow. Wall pressure and coherent structures in a turbulent boundary layer on a cylinder in axial flow. *J. Fluid Mech.*, 286:137–171, 1995.

[27] G. Spedding and P. Meunier. Momentumless and almost-momentumless wakes in a stratified fluid. In *56th Annual Meeting of the Division of Fluid Dynamics*, New Jersey, 2003. American Physical Society.

[28] Robert J. Urich. *Principles of underwater sound*. McGraw-Hill Book Company, 1982. ISBN 0–07–066087–5.

[29] S. I. Voropayev, G. B. McEachern, H. J. S. Fernando, and D. L. Boyer. large vortex structures behind a maneuvering body in stratified fluids. *Phys. Fluids*, 11:1682, 1999.

[30] W. W. Willmarth. Pressure fluctuations beneath turbulent boundary layers. *Ann. Rev. Fluid. Mech*, 7:13–38, 1975.

[31] W. W. Willmarth, R. E. Winkel, L. K. Sharma, and T. J. Bogar. Axially symmetric turbulent boundary layers on cylinders: mean velocity profiles and wall pressure fluctuations. *J. Fluid. Mech*, 70(1):35–64, 1976.